Superconductivity in aligned laminar composites

C. R. Spencer, Piero Martinoli, E. D. Gibson, J. D. Verhoeven, and D. K. Finnemore
Ames Laboratory–Department of Energy and Department of Physics, Iowa State University, Ames, Iowa 50011
(Received 27 December 1977)

Long ribbons of oriented lamellar superconductor-normal composites have been prepared by a high-speed directional solidification technique. Typically the samples are composed of 5000 alternating superconducting and normal-metal layers in which the pair potential is modulated with an amplitude of half the bulk superconductor pair potential value. By controlling the growth rate, the period of modulation can be selected to be any value in the range 5000–90000 Å. Studies of flux pinning and flux flow are reported for transport currents both parallel and perpendicular to the layers. For vortex motion parallel to the layers, flux enters the normal-metal region of the specimen and moves across the specimen at current densities on the order of 100 A/cm^2. For vortex motion perpendicular to the layers, there is no flux flow until current densities are on the order of 50000 A/cm^2. Hence, the anisotropy in critical current is approximately a factor of 500.

I. INTRODUCTION

Lamellar eutectic composites[1-3] in which all of the lamellas are aligned provide an excellent model system for the study of flux pinning in superconductors. The materials have a well-defined rectilinear geometry and many of the fundamental parameters, such as the lamellar repeat distance (d), the penetration depth (λ), the coherence distances (ξ), and the electron mean-free path (l), can be systematically varied. In addition, the boundaries are cleanly defined and the change in pair potential is rather sharp at the boundary.[4-6] By carefully controlling the heat flow during solidification, these composites can be prepared reproducibly so that all of the layers are parallel to one another and extend across the full dimension of the sample. Ribbons which are 20μm thick by 1 cm wide by 4 cm long can be prepared with any desired repeat distance ranging from 5000 to 90 000 Å.

The phase diagram of Pb-Cd has a eutectic point at Cd–72-at.%-Pb and all the samples reported here were grown at the eutectic composition. From this composition and the known molar volumes,[5] the thickness of the Pb layers is found to be 3.6 times the thickness of the Cd. Hence, a sample with a repeat distance (d) of 5000 Å will have a Cd thickness (d_N) of 1090 Å and a Pb thickness (d_S) of 3910 Å. The solubility of Cd in the Pb at the melting temperature is about 5% but this solubility decreases quickly to about 1.4% at room temperature. This typically gives an electronic mean-free path of a few hundred angstroms in the Pb regions in the normal state. By annealing the sample at room temperature for several weeks, the Cd will precipitate out of the Pb and this gives some control over the mean-free path. The solubility of the Pb in Cd is much lower, about 0.14% at the melting point, and the electronic mean-free path in the Cd is much longer than in the Pb, typically 30 000 Å. Hence the Cd layers are always in the clean limit whereas the Pb layers can be prepared as either a type I or type II superconductor depending on the annealing time.

A number of investigations of the proximity effect in the Pb-Cd system have been reported and several features of the spatial dependence of the pair potential are known. Bevolo and co-workers[5] used measurements of the jump in specific heat at T_c for bulk lamellar eutectics in conjunction with the theory of Fulde and Moorman[7] to show that the pair potential remains rather large throughout the Cd regions. Indeed they found a smaller spatial variation in the pair potential than Lechevet and co-workers[3] found for the Pb-Sn system. In a thin-film experiment, Toplicar and Finnemore[4] have used electron tunneling to study bilayer composites of Pb-Cd prepared by evaporation. At energies near the gap edge (1 meV) the tunneling density of states agrees fairly well with the McMillan tunneling model[8] for the proximity effect in all of the essential features, although there are distinct quantitative differences. At higher energies, in the region of the phonon-induced structure (3–10 meV), the tunneling density of states for injection into the superconducting side of the sandwich shows phonon structure similar to the bulk for Pb thickness as small as 300 Å. The electron-phonon coupling constant $\lambda_{ep} = \int [2\alpha^2 F(\omega)\, d\omega/\omega]$ is essentially unchanged from the bulk and the decrease in T_c can be described by a lifetime effect for electrons escaping into the Cd region. A full theory for the decrease in T_c, however, is still not available. Results for tunneling into the Cd side of the bilayers show[4] that the minimum pair potential for the composite bilayer for electrons injected perpendicular to the

layers is always somewhat larger than that predicted by the de Gennes[6] boundary condition $\Delta_1/N_1V_1 = \Delta_2/N_2V_2$, where Δ is the pair potential, N is the density of states, V is the interaction energy, and the subscripts designate the respective metals. For example, a bilayer with 500 Å of Pb and 1200 Å of Cd has a minimum value of the pair potential for the composite at the back edge of the Cd which is about 50% of pair potential on the front edge of the Pb.[4] It is important to remember, however, that tunneling quasiparticles have a rather small acceptance angle so the injected electrons predominantly go into states with momentum perpendicular to the layers. These states should have a larger pair potential[9] than de Gennes[6] predicts.

Further information about the pair potential has come from transport measurements. Migliori and Ginsberg[10] showed that the thermal conductivity of evaporated thin-film proximity bilayers of In-Tl could be fit with an effective-gap model and de Gennes boundary conditions. In addition, Deutscher and co-workers[11] have used bilayers and triple layers of the PbBi-Ag system to study the electron-electron interaction NV, and to determine the energy gap for different types of scattering at the interface. More recently, Zaitlin[12] has used thermal-conductivity measurements in aligned lamellar eutectic composites with approximately 5000 layers to study the pair potential in the normal-metal region. He finds that Δ/NV is continuous at the boundary for the clean limit and in addition finds that the pair potential in the normal metal is essentially independent of thickness at very low temperatures where the decay of Δ in the normal metal is very slow. Pb-Cd obeys many aspects of the theory and seems to be a good combination for the study of flux pinning at a metal-metal boundary.

The purpose of this series of measurements is to build model systems in which fluxoid structures and flux pinning can be studied for planar interfaces which have a sharp rise in the pair potential at the interface. These lammar systems yield information of technological importance in addition to their fundamental interest. We report here the details of sample preparation, the results of preliminary flux-pinning studies.

II. SAMPLE PREPARATION

Proper control of heat flow[1,13] is the essential ingredient for the preparation of oriented lamellar eutectics of large dimension. In this work the growth of the eutectics is based on the same principles as in the pioneering work of DuPart, Baixeras, and co-workers[1] but some modifications have been made to permit better control of the heat flow.[13]

Directional solidification of these composites was carried out in a stainless-steel parallelepiped which was constructed from commercial 304 stainless tubing. A tube with 1.11-cm outer diameter, 0.051-cm wall thickness, and 20-cm length was partially flattened and a piece of 0.025 cm thick Cu sheet was inserted into the tube. The stainless-copper sandwich was then flattened to about 1.25 mm in a rolling mill and the copper was removed with 50-vol%-nitric-acid-water solution. The resulting hollow parallelepiped was cleaned, sealed in a quartz tube under vacuum and annealed for $\frac{1}{2}$ h at 1100 °C to remove the strains developed from the cold rolling.

A flattened sheet of eutectic Pb-Cd alloy was then coated with a graphite-methanol solution and inserted into the stainless tube using 0.0025-cm feeler stock as a pulling device. It is important that the Pb-Cd fill the stainless tube fairly well to reduce the void formation. The tube was inserted into a vacuum chamber which had provision for heliarc welding. One end of the stainless tube was then arc-welded shut under a helium atmosphere of about 600 Torr. The weld was ground smooth and the composite rolled to a thickness of about 30 μm, exercising care not to over roll the sample. This is a delicate part of the procedure because it is important to completely fill the stainless without bursting it. A 0.02-cm-diam hole was drilled in one end served as an attachment device in solidification apparatus. Both the end of the tube and hole were then sealed with Dow Corning 732 RTV silicone rubber or they were heliarc-welded shut.

The drive mechanism for the directional solidification is shown in Fig. 1. In this apparatus a steep temperature gradient is maintained on one end of the furnace by a stream of cooling water directed at the sample. Neoprene "O" rings are used to control the flow of water. The furnace cooling water assembly is moved very steadily along the sample by an oscillator-driven motor so that the liquid-solid interface with a steep temperature gradient slowly moves along the length of the sample.

After the directional solidification run was completed, the ends and edges of the stainless were carefully removed with a sheet metal shear. This exposed the solidified duplex structure in the form of a foil covered with graphite. Typically there will be lengths several cm long which are well formed samples and other lacy regions where the sample did not completely fill the tube. The graphite could be removed by carefully swabbing and ultrasonically cleaning in methanol. The de-

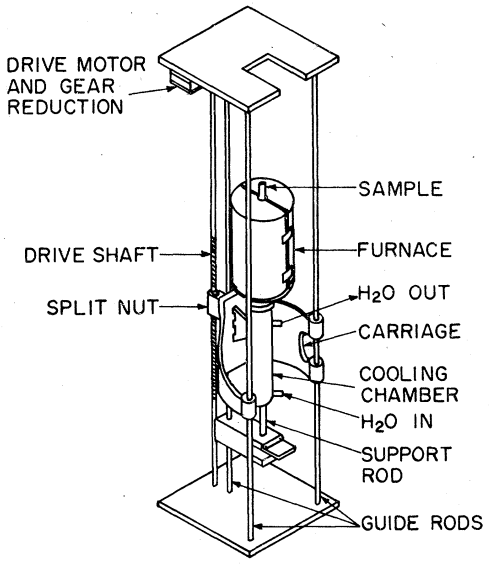

FIG. 1. Experimental apparatus for directional solidification.

sired shape for the specimen was cut with a razor blade using a small steel straight edge as a guide. The cutting operation badly damaged the edges of the sample and this portion was removed by electropolishing. To do this, microstop lacquer was painted over all areas except the edges and the sample was polished in a 1-vol% perchloric acid-methanol bath maintained at $-60\,^{\circ}C$. Typical polishing parameters were $1-1\frac{1}{2}$ min at 30 V and 1.5 A/cm^2. Edges were examined in a microscope to ascertain that the damaged areas had indeed been removed. The microstop lacquer was removed by ultrasonic cleaning in acetone. Each broad surface was then remasked, in turn, as the other broad surface carefully was polished using 5-sec intervals between examinations for defects.

In order to make electrical measurements, the sample was mounted on a glass substrate by soldering to indium tabs which previously had been mounted on the glass. To control the heat during soldering it was essential to place copper heat sinks on the sample to protect those portions which had to be kept cool. A Variac was used to control the temperature of the soldering iron. A small drop of indalloy flux No. 4 was applied and the soldering iron was lowered to the sample with a drop of indium on the tip. Scanning electron microscope (SEM) micrographs, Fig. 2, revealed that the lamellar structure of the sample remained undisturbed except for the region within a few tenths of a millimeter of the solder joint. The solder contacts were found to be much more satisfactory than silver-paint contacts.

Lamellar structure, shown on the micrograph of Fig. 2, was demonstrated to be a single grain by moving the sample across the beam of the SEM. The samples are very regular. The repeat distance (d), measured in the SEM, was found to be inversely proportional to the square root of the rate (R) at which the solid-liquid interface

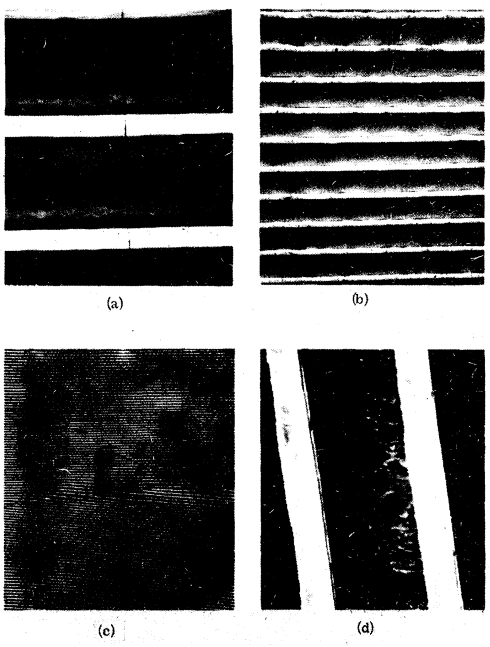

FIG. 2. Scanning electron microscope pictures of the directionally solidified Pb-Cd. Cd layers are 1000 Å thick and the Pb layers are about 5000 Å thick.

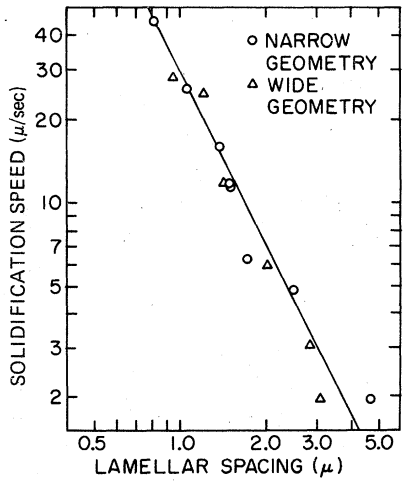

FIG. 3. Relation between the lamellar spacing and the growth rate. The solid line is $d = 500R^{-1/2}$, where d is in Å and R is in cm/sec.

moves during growth. Figure 3 shows that all of the runs obey a rule of the form

$$d = 500R^{-1/2},$$

where d is in angstroms and R is in cm/sec. To produce values of d in the range of a few thousand angstroms the rate of directional solidification is indeed rather high, a few mm/sec. More complete details of sample preparation are described elsewhere.[14]

III. EXPERIMENTAL

Two different configurations of sample were used to investigate the transport properties. Figure 4(a) illustrates the geometry used for the vortex pinning measurements in which both the current J and applied field H are parallel to the lamellas but perpendicular to one another. Figure 4(b) illustrates the geometry used to study Josephson tunneling in which the current was perpendicular to the lamella. Temperatures were measured with a calibrated germanium thermometer GR20601 or GR1592 and voltages were measured either with a photocell galvonometer or a superconducting quantum interference device (SQUID) depending on the voltage range required. Magnetic fields for the flux flow measurements were produced by a Systron-Donner alpha magnet with 28-cm-diam pole pieces and measured with a Rawson type 720 rotating-coil gaussmeter. Magnetic fields for the geometry with J perpendicular to the lamellas were produced by a superconducting coil built locally. Temperatures down to 0.3 K were generated in a ^{3}He refrigerator.

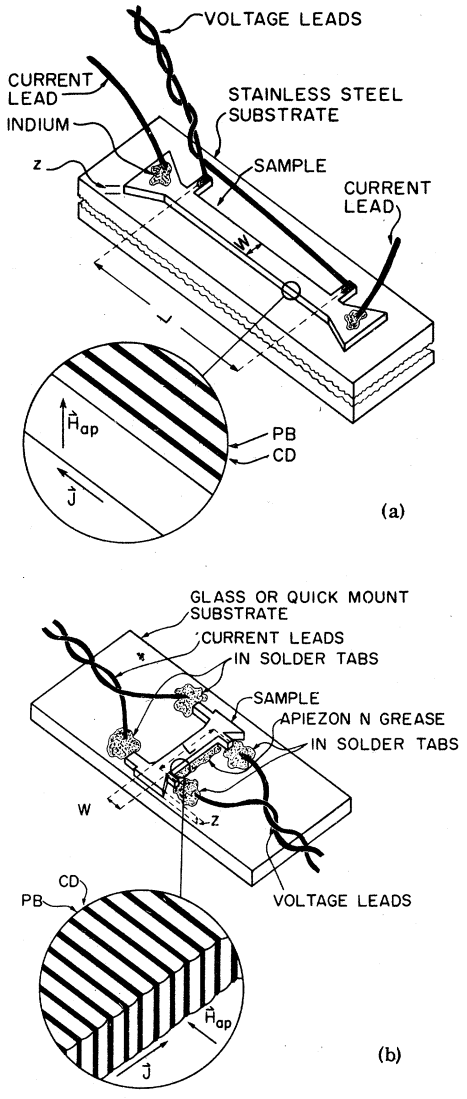

FIG. 4. Sample configurations (a) current parallel to lamellas (b) current perpendicular to lamellas.

IV. RESULTS AND DISCUSSION

A. Sample quality

The SEM micrographs are the best evidence that the samples are well-oriented lamellar composites which are uniform throughout the specimen. As long as the thickness of the foil is maintained in the 0.001–0.002-cm range, the lamellas grow perpendicular to the flat surface of the ribbon and parallel to the direction of heat flow during solidification. The SEM pictures show that the interface is smooth and sharp within the resolution of the microscope (10 Å). In addition, electron-channeling measurements indicate that the lamellas are aligned to about 1°. Sample preparation experiments conducted here indicate that 0.5 μm is about the minimum lamellar period (this gives a Cd thickness of ~1000 Å) which can be achieved with this apparatus. Faster solidification rates give lamellas oriented at an acute angle to the broad surface. Lamellar periods greater than 9 μm were not achieved because the drive mechanism on the furnace became somewhat erratic, presumably due to friction. With thinner specimens and a better drive mechanism, these limits could probably be extended.

The most serious defect in the samples was the appearance of Cd precipitates in the Pb regions if the samples were allowed to anneal at room temperature for several days. An example of this is shown in the SEM micrograph of Fig. 2(d) by the "light" structure in the otherwise "dark" Pb-rich region. Because of this precipitation, the samples were stored under liquid nitrogen unless annealing was desired. Typically a sample was grown, prepared for measurement, and cooled

to liquid-nitrogen temperature with only a few hours of annealing at room temperature. Figure 2(a) illustrates such a sample. The precipitates were a problem only after an extended anneal.

B. Characteristic lengths

The electrical resistivity of the Pb regions (ρ_{Pb}) is much higher than the Cd regions (ρ_{Cd}) because the solubility of Cd in Pb is much higher than the solubility of Pb in Cd. With this large difference the resistivity of the two phases can be determined by measuring the resistivity both parallel and perpendicular to the lamellas. For the parallel configuration the Cd layers make the dominant contribution to the conductivity and the Pb layers give a small correction. For the perpendicular direction, the Pb regions dominate the resistivity and the Cd layers make only a small correction. With these two measurements, ρ_{Cd} and ρ_{Pb} can be determined. Using the known value of ρl for Pb,[15] the mean-free path, l_{Pb}, is found to range from 500 to 3000 Å depending upon the annealing history of the sample. Because $l_{Pb} \ll d_{Pb}$, we conclude that

TABLE I. (a) Summary of parameters, J parallel to lamina.

Sample	CRS-29	CRS-28	CRS-26	CRS-27	CRS-30	CRS-33	CRS-34
d (μm)	0.65	0.985	1.46	2.53	3.00	inf.	inf.
d_{Pb}(μ m)	0.51	0.772	1.14	1.98	2.35	inf.	inf.
d_{Cd}(μm)	0.14	0.213	0.32	0.55	0.65	0.0	0.0
Anneal			No.	No.	No.		
$R_{Pb\text{-}Cd}$ (mΩ)			1.42	2.29	2.06		
$P_{Pb\text{-}Cd}$ ($\mu\Omega$ - cm)			0.287	0.256	0.370		
J_c (10^4 A/cm^2)			6.0	7.12	6.93		
H_{c2}^* (kOe)			1.34	1.46	0.44		
Anneal	2 Weeks	2 Weeks	2 Weeks	2 Weeks	2 Weeks	2 Weeks	2 Weeks
$R_{Pb\text{-}Cd}$ (mΩ)	14.91	4.24	0.88	1.73	1.24	0.040	0.072
$P_{Pb\text{-}Cd}$ ($\mu\Omega$ - cm)	0.67	0.45	0.18	0.19	0.22	0.0063	0.0070
J_c (10^4 A/cm^2)	5.86	8.88	5.13	6.33	5.38	3.99	4.18
H_{c2}^* (kOe)	0.78	0.72	1.20	0.60	0.66	0.50	0.50

(b) Summary of parameters, J perpendicular to lamina.

Sample	CRS-12	CRS-11	CRS-10	CRS-15	CRS-13	CRS-31	CRS-32
d (μ m)	0.947	1.45	2.05	2.89	3.11	9.07	9.07
d_{Pb} (μ m)	0.742	1.14	1.61	2.27	2.44	7.11	7.11
d_{Cd} (μ m)	0.205	0.31	0.44	0.62	0.67	1.96	1.96
Anneal	No.	No.	No.	No.	No.	2 Weeks	2 Months
T_c (K)	7.075	7.108	7.132	7.137	7.138	7.150	7.149
P_{Pb} ($\mu\Omega$- cm)	1.79	2.07	1.76	2.68	2.24	0.59	0.33
P_{Cd} ($\mu\Omega$ - cm)	0.056	0.056	0.056	0.056	0.056	0.056	0.056
l_{Pb} (Å)	593	513	602	395	474	1785	3202
l_{Cd} (μm)	3.125	3.125	3.125	3.125	3.125	3.125	3.125
λ_{Pb} (Å)	813	849	810	922	870	636	589
ξ_{Pb} (Å)	355	340	356	313	332	454	491
ξ_{Cd} (Å)	1378	1378	1378	1378	1378	1378	1378
ξ_{Cd} (Å)	2297	2297	2297	2297	2297	2297	2297
η	1.35	1.47	1.34	1.73	1.54	0.72	0.61

point-defect scattering from dissolved Cd is the dominant scattering mechanism in the Pb lamina. On the other hand, l_{Cd} is found to be much larger than d_{Cd} so one expects a considerable boundary scattering if the N-S interface shows diffuse scattering. No evidence of this boundary scattering has been found in this experiment, ρ_{Cd} being independent of d_{Cd}. Accordingly, we conclude that the Pb-Cd interfaces scatter specularly. This result is interpreted as evidence for N-S boundaries which are smooth on a scale comparable with the electronic wavelength.

This long-mean-free path in the Cd was somewhat unexpected so a series of Cd-rich Cd-Pb specimens were quench cast without directional solidification and the resistivity was measured in order to compare these values with the composites. Results showed a resistivity increase of 0.12 $\mu\Omega$ cm/wt. % of Pb. Hence it is quite reasonable that the Cd regions of the lamellar eutectic have a resistivity of 0.03–0.05 $\mu\Omega$ cm because the solubility of Pb in Cd is less than 0.2 wt.%.

Values for several parameters can be calculated from the mean-free path. The penetration depth is given approximately by[6] $\lambda = \lambda_L(\xi_0/l)^{1/2}$, where $\xi_L = 370$ Å and $\xi_0 = 830$ Å. The coherence distance is given by $\xi = (\xi_0 l/3)^{1/2}$. A summary of the parameters for these samples is given in Table I.

For the unannealed specimens, ρ_{Pb} was consistently about 2 $\mu\Omega$ cm giving a mean-free path of 400–600 Å. All of these samples are type II with kappa values ($\kappa \equiv H_{c2}/\sqrt{2}H_c$) of about 1.7 when they are first prepared. After a lengthy anneal the resistivity drops to about 0.5 $\mu\Omega$ cm and the sample becomes type I or type II with kappa values close to $2^{-1/2}$.

An attempt was made to measure the scattering associated with the Pb-Cd boundaries by measuring the resistivity of the composites perpendicular to the layers as a function of the repeat distance. No definitive answer could be obtained, however, because the amount of Cd in solution in the lead region could not be controlled adequately and the values of ρ_{Pb} were simply too large.

C. Superconducting properties

The transition temperature of the composite T_C is depressed in a very regular manner below the bulk superconductor T_{CB} with the reduction in the lamellar repeat distance as shown by Fig. 5. The values of T_C in the large repeat distance limit T_{CB} is below the 7.22 value of pure Pb because about 1-at.% Cd is dissolved in the Pb. On the basis of specific-heat measurements of a quenched alloy[5] one expects a T_{CB} value of about

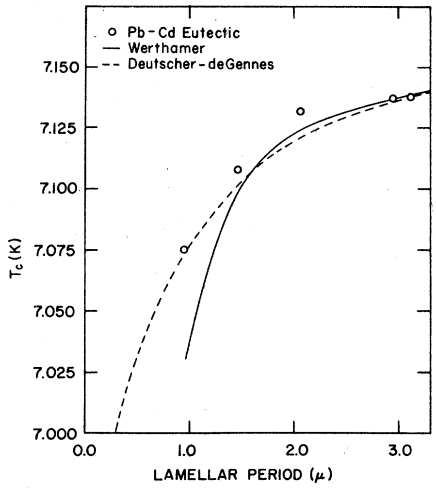

FIG. 5. Dependence of T_C on lamellar period.

7.15 K and this is close to the observations for these composites. Theoretical calculations for both the Werthamer[16] and the Deutscher–de Gennes[17] theories are shown for comparison. A fit of the data to the Deutscher–de Gennes theory give $T_{CB} = 7.16$ in good agreement with the previous specific-heat result. There are too many variables changing from sample to sample (d_S, d_N, l) to provide a good test of the theory and it is not our goal here to make such a test. The intent in Fig. 5 is simply to show that the general behavior of the data is similar to the theory.

For all of these composites, the values of d_S are very large and one can evaluate the extrapolation length (b) for the wave function (ψ) at the boundary, $\psi/b = (\partial\psi/\partial x)_{x=0}$, from the relation[17]

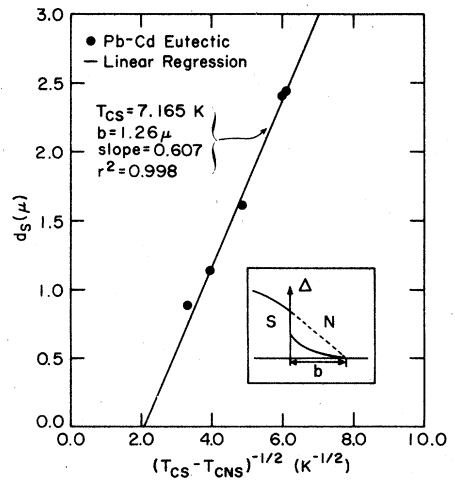

FIG. 6. Plot to determine the extrapolation length b for these composites.

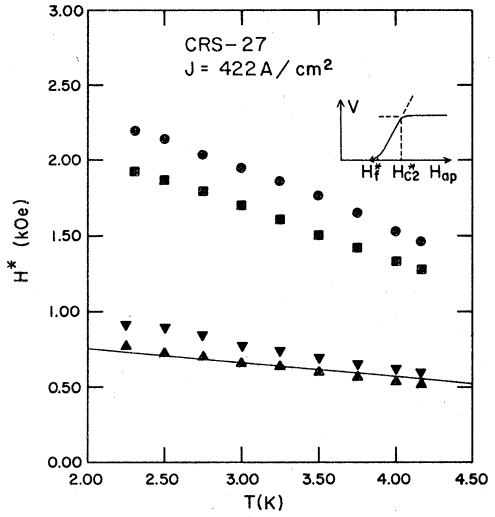

FIG. 7. Critical field curves for Pb-Cd eutectic. After an anneal at room temperature for a week, the sample reverts to type I behavior. Circles are unannealed sample. Triangles are after 2-week anneal.

$$T_{CB} - T_C = \text{const}(d_S + b)^{-2}.$$

A plot of d_S vs $(T_{CB} - T_C)^{-1/2}$ gives a reasonably straight line with an extrapolation length of 12 600 Å and $T_{CB} = 7.165$ as shown in Fig. 6.

The upper critical field for these composites is rather sensitive to the state of anneal because the mean-free path changes markedly. As shown in Fig. 7, the unannealed specimens have an H_{c2} of about 2000 Oe and the annealed specimens drop very close to the pure Pb value shown by the solid line. Hence the composites can be prepared in a variety of purity states by controling the anneal time.

D. Pinning and flux flow

Critical current measurements were made in the geometry shown in Fig. 4(a) with the current parallel to the lamellas and the vortex motion perpendicular to the lamellas. The V vs I characteristics, illustrated on Fig. 8(a), show lossless behavior up to a critical depinning current and flux-flow behavior at higher currents. Typical values of the depinning current I_C are 40 A, which corresponds to a depinning current density of $J_C = 6 \times 10^4$ A/cm at 4.2 K. These values are well above the critical currents calculated as follows using the Silsbee criterion.[20] Huebener, Kampwirth, and Clem[18] have shown that a transport current I will produce a field H_c at the edge of a wide, thin, type I superconducting strip

$$H_c = 0.4\, I / L_y,$$

where L_y is the thickness of the strip in cm, I is the current in A, and H_c is the field in G. For a type II sample flux will enter at a lower current. Hence the Silsbee criterion would predict flux entry for currents less than 5 A at 4.2 K for these samples. This is far below the measured critical currents.

A critical state model[19] can be used to explain the absence of a voltage at currents in excess of the above Silsbee criterion[20] prediction. For example, sample CRS-30, shown in Fig. 8(a), in the absence of an applied field would exclude all the flux up to a current of about 5 A. At this current, flux would begin to enter the specimen near both the edges but bulk pinning forces, describable by a critical-state current density, would prevent the flux from moving across the specimen. As the current is raised further, the flux fronts move towards each other and reach the center at a current of 44 A. When the flux fronts reach the center, vortices of opposite sense annihilate and flux flow begins. If one makes the assumption that the critical-state current density is inde-

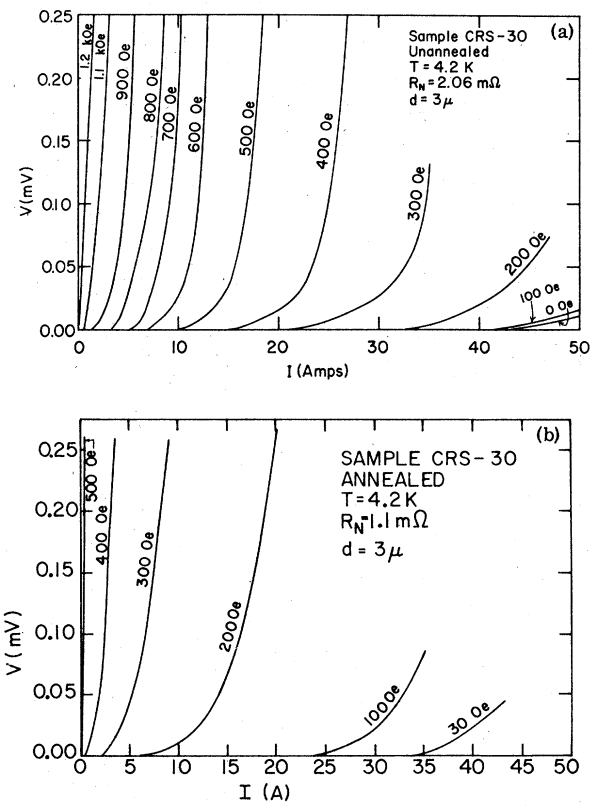

FIG. 8. Current-voltage measurements for the current parallel to the lamellas configuration. Above a critical depinning current, flux flow begins. (a) Unannealed. (b) Annealed at room temperature for 2 weeks.

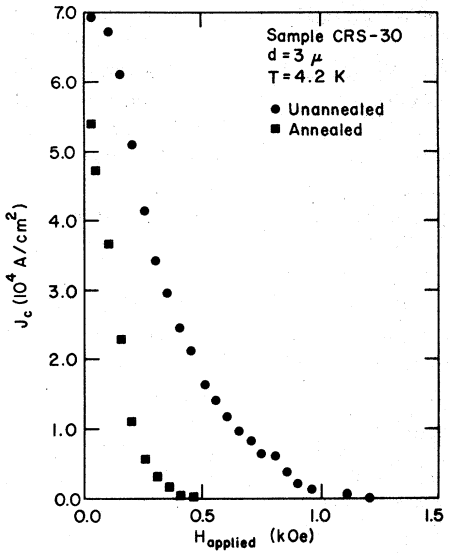

FIG. 9. Magnetic field dependence of critical currents.

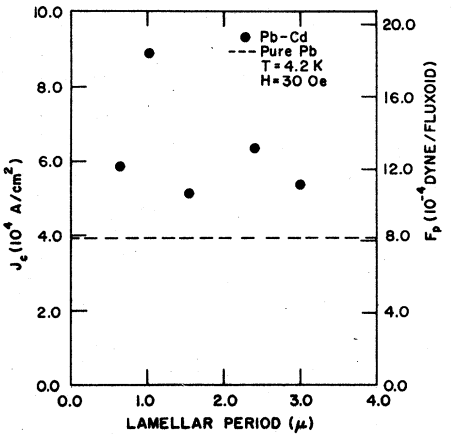

FIG. 10. Variation in critical current with lamellar repeat distance. In this regime where d is much larger than λ at ξ, J_c is independent of d. The right-hand scale gives the pinning force.

pendent of magnetic induction B, as was done by Bean,[19] then this current density is uniform across the specimen and the critical-state shielding current density would be 6×10^4 A/cm^2.

In the presence of an applied magnetic field, the critical current is found experimentally to drop with a characteristic "bell" shape curve which goes to zero at H_{c2}. The general shape of the curve is approximately the same for all samples providing the magnetic field axis is scaled by H_{c2}.

Annealing studies were carried out for a number of samples with results similar to those shown in Fig. 9. The primary effect is to lengthen the normal-state electron mean-free path in the Pb. Typically a two-week anneal will reduce ρ_{Pb} by a factor of 2 and H_{c2} decreases by a corresponding amount. The value of $J_c(H=0)$ is affected relatively little by the anneal in that it decreases by about 15%. As shown by the V vs I characteristics of Fig. 8(b) and the J_c values of Fig. 9, the primary change in the flux pinning and the flux-flow behavior can be expressed by scaling the magnetic field.

A study was made of the variation of J_c with lamellar period (d) in the range from $d=0.65$ to $d=3.0$ μm. For the unannealed samples shown in Fig. 10, J_c is about $5-6\times10^4$ A/cm^2 for all values of d and no systematic variation could be found. Within the reproducibility of the measurements, J_c is independent of d for this range. Much smaller repeat distances would be required to get a matching effect between the size of the vortex and the Cd thickness.

It has been known for some time that vacuum-metal boundaries inhibit flux entry and that, because of edge pinning, type I superconducting strips can carry currents much larger than the critical current expected from the Silsbee criterion.[21] In order to compare this effect with the superconductor–normal-metal boundary pinning, two samples of pure Pb were prepared by the same directional solidification technique. Both of these samples were type I and showed J_c values of 3.99×10^4 A/cm^2. As shown in Fig. 10, this is about $\frac{1}{2}-\frac{2}{3}$ of the critical currents of the lamellar composites. Using the model worked out by Clem *et al.*,[21] the magnetic flux enters the pure Pb samples in bundles having a thickness (t) of about 30 μm.

All of the critical current measurements on Figs. 8 and 9 were taken at 4.2 K with the sample in the helium bath. If the temperature is lowered J_c increases substantially. For example, a sample with a repeat distance of 3 μm shows an increase in J_c from 6.93×10^4 A/cm^2 at 4.2 K to 11.1×10^4 A/cm^2 at 2.2 K. All of the J_c measurements follow $J_c=J_0(1-t^2)$, where $t=T/T_C$, rather well.

E. Supercurrents perpendicular to layers

For the geometry in which the transport current is passed perpendicular to the lamina as shown in Fig. 4(b), the composites form a series of superconductor–normal-metal–superconductor (S-N-S) junctions with a very strong proximity effect. All of the samples in this study will sustain a supercurrent through the Cd layers with critical currents and V-I characteristics similar to single S-N-S junctions. A typical value for the

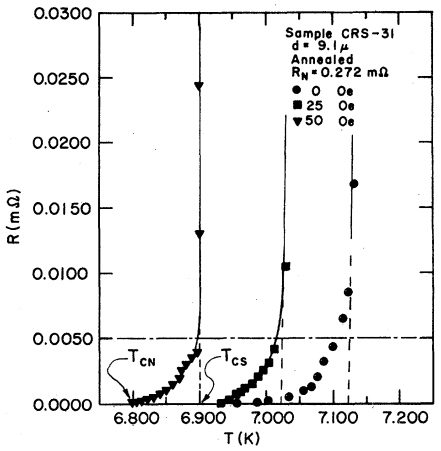

FIG. 11. Resistive transition for a Pb-Cd composite with the transport current perpendicular to the layers. The dashed line indicates the resistance of the Cd layers when they are in the normal state.

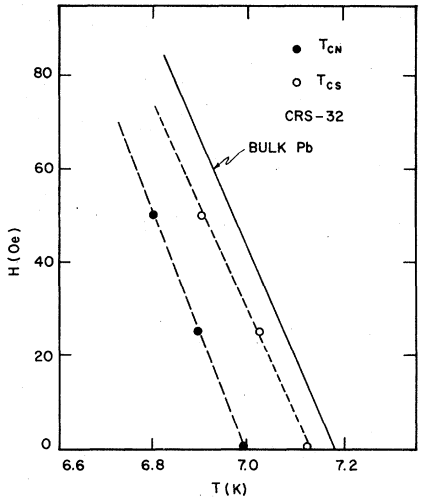

FIG. 12. Critical field curves for the superconducting (open circles) and normal (solid circles) lamellas at a measuring current density of 10 A/cm^2.

critical current is 10 A/cm^2 for a 20 000-Å-thick Cd layer.[22]

As the sample is cooled through T_C, the transition has two distinct regions as illustrated in Fig. 11 for a sample with $d_N = 2000$ Å. In zero applied field, there is a very sharp drop in resistance from 272 to 5 $\mu\Omega$ in the temperature interval from 7.150 to 7.120 K. This value of 5 $\mu\Omega$, shown by the dashed line of Fig. 11, is just the resistance of the Cd layers in the normal state. Below 7.120 K, the resistance falls much more slowly and the value of the resistance is very sensitive to the magnitude of the measuring current. For the 10-A/cm^2 current density shown on Fig. 11, the resistance drops to less than 10^{-9} Ω in a temperature interval of 0.150 K. Typical critical currents for the Cd layers were in the 10–100 A/cm^2 range.

These steps can be characterized by two temperatures, T_{CS} and T_{CN} as defined on Fig. 11. Indeed this steplike behavior in the transition persists when a magnetic field is applied and one can define a critical field curve for each step. If T_{CS} is identified as the transition step of the Pb regions and T_{CN} is identified as the transition step of the Cd regions as shown in Fig. 11, then one finds the critical-field curves of Fig. 12. Both the Pb lamellas and the Cd lamellas undergo phase transitions very close to the critical field curve of bulk Pb and a law of corresponding states holds. The value of T_{CN} depends on measuring current. For example, T_{CN} for sample CRS-32 drops from 7.060 to 7.000 K as J varies from 1 to 10 A/cm^2. For any fixed J, however, there is a well-defined critical field curve as in Fig. 12. A detailed quantitative study of this current dependence of the resistance was not undertaken because the sample was composed of 5000 S-N-S junctions which were not sufficiently identical to one another to provide a definitive result.

Flux flow plays an important role in the V-I characteristics of the perpendicular geometry as well as in the parallel geometry. In the low-voltage range, the SQUID detection system was used to take the measurements, shown on Fig. 13. Results indicate a zero-field critical current of 23 A/cm^2 and flux-flow behavior at higher cur-

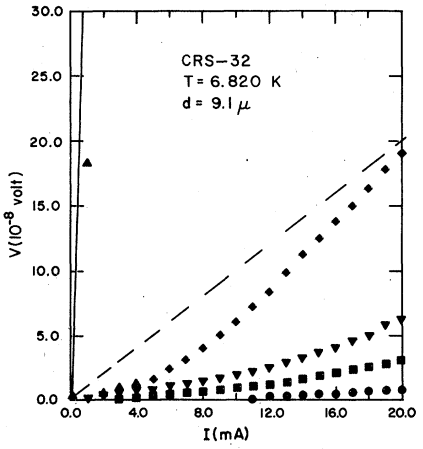

FIG. 13. V-I characteristics for vortex motion parallel to the lamellas. Dashed curve shows normal-state resistance of Cd layers. Solid curve shows resistance of Pb plus Cd layers: ● 0 Oe; ■ 20 Oe; ▽ 40 Oe; ♦ 60 Oe; ▲ 80 Oe. Dashed line shows normal-state resistance of Cd. The solid line shows normal-state resistance of Pb.

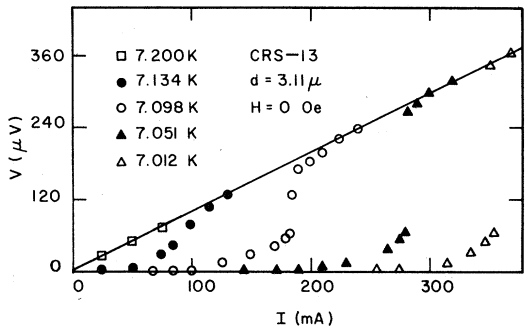

FIG. 14. Flux flow in Pb regions for vortex motion parallel to layers. Solid line shows normal-state resistivity. Note difference in voltage scales on Fig. 13 and Fig. 14.

rents. Application of a field of 20 Oe, shown by the solid squares, reduces the critical current to 12.7 A/cm^2 and substantially increases the flux-flow resistivity. The ordinate scale was chosen so that the slope corresponding to the Pb resistance, 820 $\mu\Omega$, and the Cd resistance of 20 $\mu\Omega$ could be conveniently seen. This scale, unfortunately, obscures many features. If the ordinate scale is expanded by a factor of 10 or 100, the data show a linear V-I curve with a nonzero critical current for fields up to 80 Oe. Values of the critical current as a function of magnetic field fall off roughly as expected for Josephson junctions containing several vortices.[1,23]

The flux-flow behavior undergoes an abrupt change of character at a current density of about

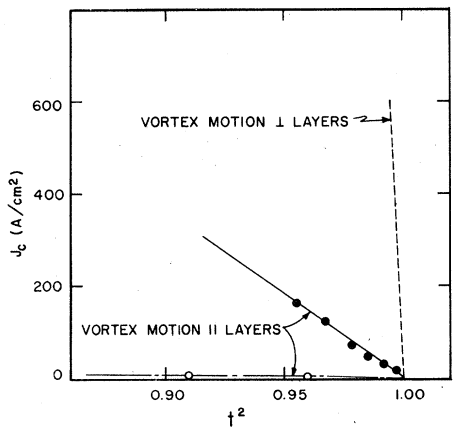

FIG. 15. Anisotropy of the critical currents for lamellar structures. J_c for vortex motion perpendicular to the layers (dashed line) is approximately 30 times J_c for vortex motion parallel to the layers. Open circles show onset of flux flow in Cd layers. Solid circles show onset of flux flow in Pb layers. $t = T/T_C$, the reduced temperature.

25 times the value at which flux flow begins in the Cd regions. The flux-flow resistivity shows a sharp increase by a factor of 100 which we associate with the onset of flux flow in the Pb regions. As shown in Fig. 14, the V vs I curves look like flux flow but the scale is rather different from Fig. 13.

For the geometry, in which the velocity of the vortices v_v is parallel to the lamellas, the temperature dependence of the critical current is of the form $J_c = J_0(1 - t^2)$ just as for the case of vortex motion perpendicular to the layers. The primary difference is that J_0 is highly anisotropic. As shown in Fig. 15, the Cd layers show flux flow (open circles) for v_v parallel to layers at a current 30 times smaller than the Pb layers (solid circles) for v_v parallel to layers. This in turn is a factor of 30 to 50 times smaller than the onset of flux flow for vortex motion perpendicular to the layers, v_v perpendicular to layers, shown by the nearly vertical dashed line of Fig. 15. For the geometry of Fig. 4(b), the Cd layers provide a weak spot where flux can enter and move at currents approximately 1000 times smaller than J_c for the geometry of Fig. 4(a). As the current is further increased in the geometry of Fig. 4(b), the Pb regions eventually enter the flux-flow state and they show flux flow at current densities which are a factor of 30 smaller than the geometry of Fig. 4(a).

V. SUMMARY

Directional solidification techniques have been developed to prepare large samples of oriented lamellar superconducting–normal-metal composites. Ribbons which are 0.002 cm by 1 cm by virtually any length can be prepared routinely by these methods. Below T_C of Pb, superconductivity is induced in the "normal" metal Cd region by the proximity effect and the sample exhibits a periodically modulated pair potential. The amplitude of the modulation is about half the magnitude of the pair potential of bulk Pb and the period of the modulation can be selected to be anywhere in the range from 5000 to 90 000 Å. As grown, the Cd regions are found to be in the clean limit (l_{Cd} ~ 30 000 Å) and the Pb regions are rather dirty (l_{Pb} ~ 600 Å). Attempts to prepare samples with a small l_{Cd} by adding Mg were only partially successful. The lamellar structures grew well for additions of 1 or 2at.% Mg but l_{Cd} remained large because Mg has such a small scattering cross section.

T_C values for the composites roughly obey the Deutscher–de Gennes model and the data indicate an extrapolation length of about 12 600 Å. The

coherence distance of Pb is about 880 Å so the pair potential in the Pb is suppressed only a few percent near the Cd boundaries. The V-I characteristics for transport currents parallel to the layers and vortex motion perpendicular to the layers [Fig. 4(a)] indicates that a critical-state model is appropriate to describe flux entry into the specimen. Critical currents are approximately 6×10^4 A/cm^2 at the onset of flux flow and the temperature dependence follows $J_c = J_0(1-t^2)$. For transport currents perpendicular to the layers, there are relatively large supercurrents (10–100 A/cm^2) through the Cd lamellas verifying that the pair potential in the center of the Cd is large. The V-I characteristics for transport currents perpendicular to the layers and vortex motion parallel to the layers [Fig. 4(b)] indicate resistive behavior at rather low currents. In this configuration critical currents are on the order of 10–100 A/cm^2 and the magnitude of the flux-flow resistivity indicates that the vortex cores are moving along the Cd layers. Values of the critical current again are proportional to $1-t^2$. As the current perpendicular to the layers continues to rise, there is a second abrupt change in the V-I characteristics when flux flow begins in the Pb regions.

The magnitude of the critical current for the onset of flux flow is highly anisotropic. For the geometry of Fig. 4(b), typical values are, for v_v parallel to layers,

$$J_c = 142(1-t^2)\ \text{A/cm}^2$$

in the Cd regions and

$$J_c = 3600(1-t^2)\ \text{A/cm}^2$$

in the Pb regions. For the geometry of Fig. 4(a), typical values are, for v_v, perpendicular to layers,

$$J_c = 82000(1-t^2)\ \text{A/cm}^2.$$

Superconductor–normal-metal boundaries with this range of spacing do not permit J_c values as large as the depairing current but they certainly impede the motion of vortices. To make further progress in this line, it is important to prepare samples with shorter mean-free paths to give a more abrupt change in pair potential. In addition, smaller dimensions are needed to match the repeat distance to λ and ξ and to prevent the suppression of the pair potential by the self-field.

ACKNOWLEDGMENTS

J. R. Clem, J. E. Ostenson, and M. P. Zaitlin have made important contributions to this work. P. Martinoli was on leave from ETH Zurich Switzerland. This work was supported by the U. S. Department of Energy, Office of Basic Energy Sciences.

[1] J. M. Dupart, J. Rosenblatt, and J. Baixeras, Phys. Rev. B 16, 4815 (1977); J. M. Dupart and J. Baixeras, Appl. Phys. Lett. 30, 123 (1977); A. Guinier, C. Petipas, G. Sauvage, J. Baixeras, J. M. Dupart, G. Fournet, G. Fontaine, M. G. Blanchin, M. Turpin, and R. Racek, Conference on In Situ Composites, Lakeville, Conn. (National Materials Advising Board, Washington, D.C., 1973), Vol. III; M. G. Blanchin, A. Guinier, C. Petipas, and G. Sauvage, Acta Metall. 20, 1251 (1972).

[2] H. Raffy, J. C. Renard, and E. Guyon, Solid State Commun. 11, 1679 (1972); H. Raffy, E. Guyon, and J. C. Renard, Solid State Commun. 14, 427 (1974); H. Raffy, E. Guyon, and J. R. Renard, Solid State Commun. 14, 431 (1974).

[3] J. Lechevet, J. E. Neighbor, and C. A. Shiffman, Phys. Rev. B 5, 861 (1972); J. Lechevet, J. E. Neighbor, and C. A. Shiffman, J. Low Temp. Phys. 27, 407 (1977).

[4] J. R. Toplicar and D. K. Finnemore, Phys. Rev. B 16, 2072 (1977); J. R. Toplicar and D. K. Finnemore, Solid State Commun. 19, 859 (1976).

[5] A. J. Bevolo, E. D. Gibson, J. D. Verhoeven, and D. K. Finnemore, Phys. Rev. B 14, 114 (1976).

[6] P. G. de Gennes, Rev. Mod. Phys. 36, 225 (1964); P. G. de Gennes, *Superconductivity in Metals and Alloys* (Benjamin, New York, 1966).

[7] P. Fulde and W. Moormann, Phys. Kondens. Mater. 6, 403 (1967).

[8] W. L. McMillan, Phys. Rev. 175, 537 (1968).

[9] D. Saint James, J. Phys. (Paris) 25, 899 (1964).

[10] A. Migliori and D. M. Ginsberg, Phys. Rev. B 8, 5065 (1973).

[11] G. Deutscher, S. Y. Hseih, P. Lindenfeld, and S. Wolf, Phys. Rev. B 8, 5055 (1973).

[12] M. Zaitlin (unpublished).

[13] J. D. Verhoeven, *Fundamentals of Physical Metallurgy* (Wiley, New York, 1975).

[14] C. R. Spencer, Ph.D. thesis (Iowa State University, 1977) (unpublished).

[15] R. G. Chambers, Proc. R. Soc. Lond. 215, 481 (1952).

[16] N. R. Werthamer, Phys. Rev. 132, 2440 (1963).

[17] G. Deutscher and P. G. de Gennes, in *Superconductivity*, edited by R. D. Parks (Dekker, New York, 1969). L. Dobrosavljevic and P. G. de Gennes, Solid State Commun. 5, 177 (1967).

[18] R. P. Huebener, R. T. Kampwirth, and J. R. Clem, J. Low Temp. Phys. 6, 275 (1972).

[19] C. P. Bean, Phys. Rev. Lett. 8, 250 (1962).

[20] F. B. Silsbee, J. Wash. Acad. Sci. 6, 427 (1916).

[21] J. Clem, R. P. Huebener, and D. E. Gallus, J. Low Temp. Phys. 12, 449 (1974).

[22] J. Clarke, Proc. R. Soc. A 308, 447 (1969).

[23] C. S. Owen and D. J. Scalapino, Phys. Rev. 164, 538 (1967); A. M. Goldman and P. J. Kreisman, Phys. Rev. 164, 544 (1967).

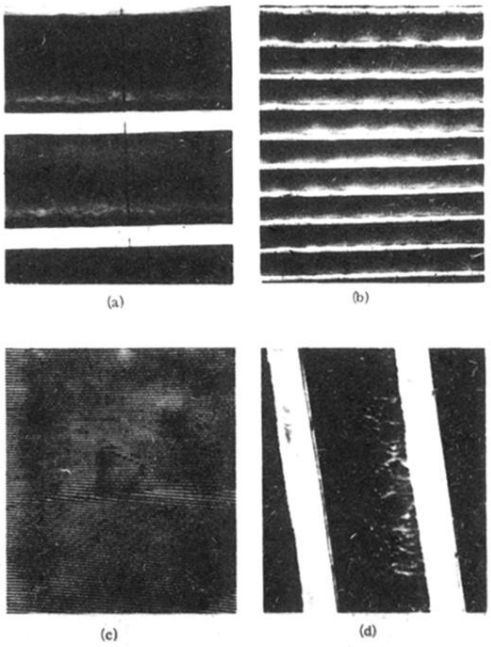

FIG. 2. Scanning electron microscope pictures of the directionally solidified Pb-Cd. Cd layers are 1000 Å thick and the Pb layers are about 5000 Å thick.